
FleXOR: Trainable Fractional Quantization

Dongsoo Lee* Se Jung Kwon* Byeongwook Kim
 Yongkweon Jeon Baeseong Park Jeongin Yun
 Samsung Research, Seoul, Republic of Korea
 {dongsoo3.lee, sejung0.kwon, byeonguk.kim,
 dragwon.jeon, bpbs.park, ji6373.yun}@samsung.com

Abstract

Quantization based on the binary codes is gaining attention because each quantized bit can be directly utilized for computations without dequantization using look-up tables. Previous attempts, however, only allow for integer numbers of quantization bits, which ends up restricting the search space for compression ratio and accuracy. In this paper, we propose an encryption algorithm/architecture to compress quantized weights so as to achieve fractional numbers of bits per weight. Decryption during inference is implemented by digital XOR-gate networks added into the neural network model while XOR gates are described by utilizing $\tanh(x)$ for backward propagation to enable gradient calculations. We perform experiments using MNIST, CIFAR-10, and ImageNet to show that inserting XOR gates learns quantization/encrypted bit decisions through training and obtains high accuracy even for fractional sub 1-bit weights. As a result, our proposed method yields smaller size and higher model accuracy compared to binary neural networks.

1 Introduction

Deep Neural Networks (DNNs) demand larger number of parameters and more computations to support various task descriptions all while adhering to ever-increasing model accuracy requirements. Because of abundant redundancy in DNN models [9, 5, 3], numerous model compression techniques are being studied to expedite inference of DNNs [21, 17]. As a practical model compression scheme, parameter quantization is a popular choice because of high compression ratio and regular formats after compression so as to enable full memory bandwidth utilization.

Quantization schemes based on binary codes are gaining increasing attention since quantized weights follow specific constraints to allow simpler computations during inference. Specifically, using the binary codes, a weight vector is represented as $\sum_{i=1}^q (\alpha_i \mathbf{b}_i)$, where q is the number of quantization bits, α is a scaling factor ($\alpha \in \mathbb{R}$), and each element of a vector \mathbf{b}_i is a binary $\in \{-1, +1\}$. Then, a dot product with activations is conducted as $\sum_{i=1}^q (\alpha_i \sum_{j=1}^v a_j b_{i,j})$, where a_j is a full-precision activation and v is the vector size. Note that the number of multiplications is reduced from v to q (expensive floating-point multipliers are less required for inference). Moreover, even though we do not discuss a new activation quantization method in this paper, if activations are also quantized by using binary codes, then most computations are replaced with bit-wise operations (using XNOR logic and population counts) [27, 22]. Consequently, even though representation space is constrained compared with quantization methods based on look-up tables, various inference accelerators can be designed to exploit advantages of binary codes [22, 27]. Since a successful 1-bit weight quantization method has been demonstrated in BinaryConnect [3], advances in compression-aware training algorithms in the form of binary codes (e.g., binary weight networks [22] and LQ-Nets [29]) produce 1-3 bits for quantization while accuracy drop is modest or negligible. Fundamental investi-

*Equal Contribution.

	Weights on MEM	Converter	Input Weight Format	Computation Scheme
Ours (FleXOR)	Encrypted W (w/ Scaling Factors)	XOR Decryptor	Binarized W	Bit-wise Computation
Binary-coding-based Quantization	Binarized W (w/ Scaling Factors)		Binarized W	Bit-wise Computation
Vector Quantization	Quantized W (w/ Codebooks)	Looking up Codebooks	W (Full Precision)	Full Precision Computation

Figure 1: Dataflow and computation formats of binary-coding-based quantization, vector quantization, and our proposed quantization scheme.

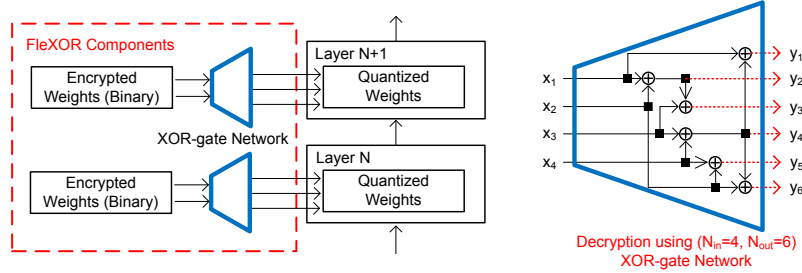


Figure 2: FleXOR components added to the quantized DNNs to compress quantized weights through encryption. Encrypted weight bits are decrypted by XOR gates to produce quantized weight bits.

gations on DNN training mechanisms using fewer quantization bits have also been actively reported [19, 2].

Previously, binary-coding-based quantization has only permitted integer numbers of quantization bits, limiting the compression/accuracy trade-off search space, especially in the range of very low quantization bits. In this paper, we propose a flexible encryption algorithm/architecture (called ‘‘FleXOR’’) to enable fractional sub 1-bit numbers to represent each weight while quantized bits are trained by gradient descent. Even though vector quantization is also a well-known scheme with high compression ratio [24], we assume the form of binary codes. Note that the number of quantization bits can be different for each layer (e.g., [26]) to allow fractional quantization bits on average. FleXOR implies fractional quantization bits for each layer that can be quantized with different bits.

To the best of our knowledge, **our work is the first to explore model accuracy under 1 bit/weight when weights are quantized based on the binary codes.** Figure 1 compares representations of weights to be stored in memory, converting method, and computation schemes of three quantization schemes. FleXOR maintains the advantages of binary-coding-based quantization (i.e., dequantization is not necessary for the computations) while quantized weights are further compressed by encryption.

2 Encrypting Quantized Bits using XOR Gates

The main purpose of FleXOR is to compress quantized bits into encrypted bits that can be reconstructed by XOR gates as shown in Figure 2. Suppose that N_{out} bits are to be compressed into N_{in} bits ($N_{out} > N_{in}$). The role of an XOR-gate network is to produce various N_{out} -bit combinations using N_{in} bits [15]. In other words, in order to maximize the chance of generating a desirable set of quantized bits, the encryption scheme is designed to seek a particular property where all possible $2^{N_{in}}$ outcomes through decryption are evenly distributed in $2^{N_{out}}$ space.

A linear Boolean function, $f(\mathbf{x})$, maps $f : \{0, 1\}^{N_{in}} \rightarrow \{0, 1\}$ and has the form of $a_1x_1 \oplus a_2x_2 \oplus \dots \oplus a_{N_{in}}x_{N_{in}}$ where $a_j \in \{0, 1\}$ ($1 \leq j \leq N_{in}$) and \oplus indicates bit-wise modulo-2 addition. In Figure 2, six binary outputs are generated through six Boolean functions using four binary inputs. Let $f_1(\mathbf{x})$ and $f_2(\mathbf{x})$ be two such linear Boolean functions using $\mathbf{x} = (x_1, x_2, \dots, x_{N_{in}}) \in \{0, 1\}^{N_{in}}$. The Hamming distance between $f_1(\mathbf{x})$ and $f_2(\mathbf{x})$ is the number of inputs on which $f_1(\mathbf{x})$ and $f_2(\mathbf{x})$

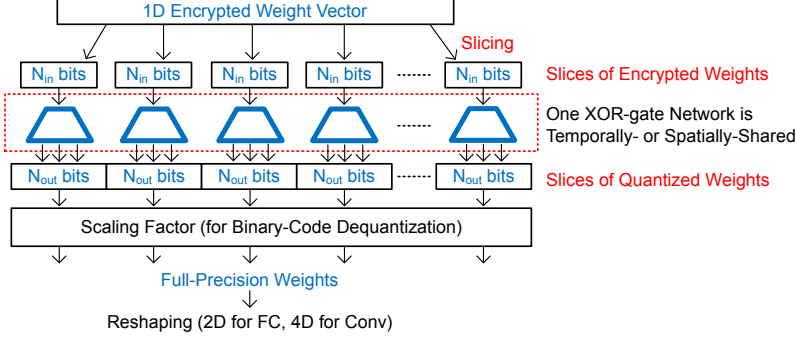


Figure 3: Encrypted weight bits are sliced and reconstructed by a XOR-gate network which can be shared (in time or space). Then quantized bits after XOR gates are finally reshaped.

differ, and defined as

$$d_H(f_1, f_2) := w_H(f_1 \oplus f_2) = \#\{\mathbf{x} \in \{0, 1\}^{N_{in}} | f_1(\mathbf{x}) \neq f_2(\mathbf{x})\}, \quad (1)$$

where $w_H(f) = \#\{\mathbf{x} \in \{0, 1\}^{N_{in}} | f(\mathbf{x}) = 1\}$ is the Hamming weight of a function and $\#\{\}$ corresponds to the size of a set [13]. The Hamming distance is a well-known method to express non-linearity between two Boolean functions [13] and increased Hamming distance between a pair of two Boolean functions results in a variety of outputs produced by XOR gates. Increasing Hamming distance is a required feature for cryptography to derive complicated encryption structure such that inverting encrypted data becomes difficult. For digital communication, the Hamming distance between encoded signals is closely related to the amount of error correction possible.

In Figure 2, y_1 is represented as $x_1 \oplus x_3 \oplus x_4$, or equivalently a vector $[1\ 0\ 1\ 1]$ denoting which inputs are selected. Concatenating such vectors, a XOR-gate network in Figure 2 can be described as a binary matrix $M^\oplus \in \{0, 1\}^{N_{out} \times N_{in}}$ (e.g., the second row of M^\oplus is $[1\ 1\ 0\ 0]$ and the third row is $[1\ 1\ 1\ 0]$). Then, decryption through XOR gates is simply represented as $\mathbf{y} = M^\oplus \mathbf{x}$ where \mathbf{x} and \mathbf{y} are the binary inputs and binary outputs of XOR gates, and addition is ‘XOR’ and multiplication is ‘AND’ (see Appendix for more details and examples).

Encrypted weight bits are stored in 1-dimensional vector format and sliced into blocks of N_{in} -bit size as shown in Figure 3. Then, decryption of each slice is performed by a XOR-gate network that is shared by all slices (temporally- or spatially-shared). Depending on the quantization scheme and characteristics of layers, quantized bits may need to be scaled by a scaling factor and/or reshaped. Area and latency overhead induced by XOR gates are negligible as demonstrated in VLSI testing and parameter pruning works [25, 17, 1].

3 FleXOR Training Algorithm for Quantization Bits Decision

Once the structure of XOR gates has been pre-determined and fixed to increase the Hamming distance of XOR outputs, we find quantized and encrypted bits by adding XOR gates into the model. In other words, we want an optimizer that understands the XOR-gate network structure so as to compute encrypted bits and scaling factors via gradient descent. For inference, we store binary encrypted weights (converted from real number encrypted weights) in memory and generate binary quantized weights through Boolean XOR operations. Activation quantization is not discussed in this paper.

Similar to the STE method introduced in [3], Boolean functions need to be described in a differentiable manner to obtain gradients in backward propagation. For two real number inputs x_1 and x_2 ($x_1, x_2 \in \mathbb{R}$ to be used as encrypted weights), the Boolean version of a XOR gate for forward propagation is described as (note that 0 is replaced with -1)

$$\mathcal{F}^\oplus(x_1, x_2) = (-1) \text{sign}(x_1) \text{sign}(x_2). \quad (2)$$

For inference, we store $\text{sign}(x_1)$ and $\text{sign}(x_2)$ instead of x_1 and x_2 . On the other hand, a differentiable XOR gate for backward propagation is presented as

$$f^\oplus(x_1, x_2) = (-1) \tanh(x_1 \cdot S_{\tanh}) \tanh(x_2 \cdot S_{\tanh}), \quad (3)$$

where S_{\tanh} is a scaling factor for FleXOR. Note that \tanh functions are widely used to approximate Heaviside step functions (i.e., $y(x)=1$ if $x>0$ or 0, otherwise) in digital signal processing and S_{\tanh} can control the steepness. In [6, 16], \tanh is also suggested to approximate the STE function. In our work, on the other hand, \tanh is proposed to make XOR operations trainable for ‘encryption,’ rather than ‘quantization.’ In the case of consecutive XOR operations, the order of inputs to be fed into XOR gates should not affect the computation of partial gradients for XOR inputs. Therefore, as a simple extension of Eq. (3), a differentiable XOR gate network with n inputs can be described as

$$f^{\oplus}(x_1, x_2, \dots, x_n) = (-1)^{n-1} \tanh(x_1 \cdot S_{\tanh}) \tanh(x_2 \cdot S_{\tanh}) \dots \tanh(x_n \cdot S_{\tanh}). \quad (4)$$

Then, a partial derivative of f^{\oplus} with respect to x_i (an encrypted weight) is given as

$$\frac{\partial f^{\oplus}(x_1, x_2, \dots, x_n)}{\partial x_i} = S_{\tanh} (-1)^{n-1} (1 - \tanh^2(x_i \cdot S_{\tanh})) \frac{\prod_{j=1}^n \tanh(x_j \cdot S_{\tanh})}{\tanh(x_i \cdot S_{\tanh})} \quad (5)$$

Note that increasing the Hamming distance is associated with more \tanh multiplications for each XOR-gate network output. Then, from Eq. (5), we may suffer from the vanishing gradient problem since $|\tanh(x)| \leq 1$. To resolve this problem, we also consider a simplified alternative partial derivative expressed as

$$\frac{\partial f^{\oplus}(x_1, x_2, \dots, x_n)}{\partial x_i} \approx S_{\tanh} (-1)^{n-1} (1 - \tanh^2(x_i \cdot S_{\tanh})) \prod_{j \neq i} \text{sign}(x_j). \quad (6)$$

Eq. (6) shows that when we compute a partial derivative, all XOR inputs other than x_i are assumed to be binary, i.e., the magnitude of a partial derivative is then only determined by x_i . We use Eq. (6) in this paper to calculate custom gradients of encrypted weights due to fast training computations and convergence, and use Eq. (2) for forward propagation.

Algorithm 1: Pseudo codes of Conv Layer with FleXOR when the kernel size is $k \times k$, the number of input channel and output channel are C_{in} and C_{out} , respectively.

$\mathbf{w}^e \in \mathbb{R}^{\lceil (k \cdot k \cdot C_{in} \cdot C_{out}) / N_{out} \rceil \cdot N_{in}}$ ▷ Encrypted weights
 $\mathbf{M}^{\oplus} \in \{0, 1\}^{N_{out} \times N_{in}}$ ▷ XOR gates (shared)
 $\alpha \in \mathbb{R}^{C_{out}}$ ▷ Scaling factors for each output channel

Function `FleXOR_Conv(input, stride, padding):`

```

for  $i \leftarrow 0$  to  $\lceil (k \cdot k \cdot C_{in} \cdot C_{out}) / N_{out} \rceil - 1$  do
  for  $j \leftarrow 1$  to  $N_{out}$  do
     $w_{i \cdot N_{out} + j}^q \leftarrow (-1) \cdot \left( \prod_{l=1, M_{j,l}^{\oplus}=1}^{N_{in}} \text{Sign}^c(w_{i \cdot N_{in} + l}^e) \cdot (-1) \right)$  ▷ Eq. (2)
   $\mathbf{W}^q \leftarrow \text{Reshape}(w^q, [k, k, C_{in}, C_{out}])$ 
  return Conv(input,  $\mathbf{W}^q$ ,  $\alpha$ , stride, padding) ▷ Conv. operation for binary codes

```

Forward Function `Signc(x):`

```

return sign(x)

```

Gradient Function `Signc(x, ∇):`

```

return  $\nabla \cdot (1 - \tanh^2(x \cdot S_{\tanh})) \cdot S_{\tanh}$  ▷ Eq. (6)

```

By training the whole network including FleXOR components using custom gradient computation methods described above, encrypted and quantized weights are obtained in a holistic manner. FleXOR operations for convolutional layers are described in Algorithm 1, where encrypted weights (inputs of a XOR-gate network) and quantized weights (outputs of a XOR-gate network) are \mathbf{w}^e and \mathbf{W}^q .

We first verify basic training principles of FleXOR using LeNet-5 on the MNIST dataset. LeNet-5 consists of two convolutional layers and two fully-connected layers (specifically, 32C5-MP2-64C5-MP2-512FC-10SoftMax), and each layer is accompanied by an XOR-gate network with N_{in} binary inputs and N_{out} binary outputs. The quantization scheme follows 1-bit binary code with full-precision scaling factors that are shared across weights for the same output channel number (for conv layers) or output neurons (for FC layers). Encrypted weights are randomly initialized with

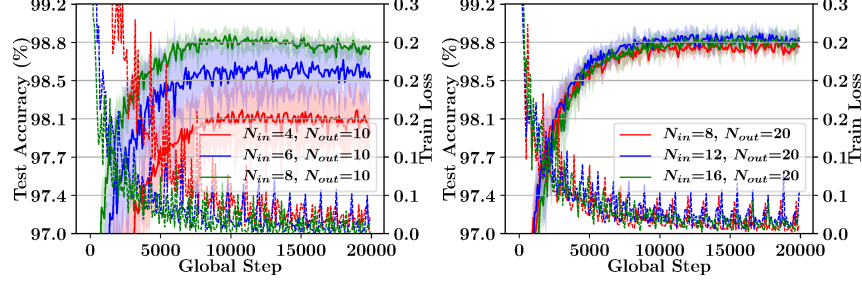


Figure 4: Test accuracy and training loss (average of 6 runs) with LeNet-5 on MNIST when M^\oplus is randomly filled with $\{0, 1\}$. N_{out} is 10 or 20 to generate 0.4, 0.6, or 0.8 bit/weight quantization.

$\mathcal{N}(\mu=0, \sigma^2=0.001^2)$. All scaling factors for quantization are initialized to be 0.2 (note that if batch normalization layers are immediately followed, then scaling factors for quantization are redundant).

Using the Adam optimizer with an initial learning rate of 10^{-4} and batch size of 50 without dropout, Figure 4 shows training loss and test accuracy when $S_{\tanh}=100$, elements of M^\oplus are randomly filled with 1 or 0, and for two values of N_{out} – 10 and 20. Using the 1-bit internal quantization method and (N_{in}, N_{out}) encryption scheme, one weight can be represented by (N_{in}/N_{out}) bits. Hence, Figure 4 represents training results for 0.4, 0.6, and 0.8 bits per weight. Note that as for a randomly filled M^\oplus , increasing N_{out} (and N_{in} is determined correspondingly for the same compression ratio) increases the Hamming distance for a pair of any two rows of M^\oplus and, hence, offers the chance to produce more diversified outputs. Indeed, as shown in Figure 4, the results for $N_{out}=20$ present improved test accuracy and less variation compared with $N_{out}=10$. See Appendix for the distribution of encrypted weights at different training steps.

4 Practical FleXOR Training Techniques

In this section, we present practical training techniques for FleXOR using ResNet-32 [10] on the CIFAR-10 dataset [14]. We show compression results for ResNet-32 using fractional numbers as effective quantization bits, such as 0.4 and 1.2, that have not been available previously.

All layers, except the first and the last layers, are followed by FleXOR components sharing the same M^\oplus structure (thus, storage footprint of M^\oplus is ignorable). SGD optimizer is used with momentum of 0.9 and a weight decay factor of 10^{-5} . Initial learning rate is 0.1, which is decayed by 0.5 at the 150th and 175th epoch. As learning rate decays, S_{\tanh} is empirically multiplied by 2 to cancel out the effects of weight decay on encrypted weights. Batch size is 128 and initial scaling factors of α are 0.2. q is the number of bits to represent binary codes for quantization. We provide some useful training insights below with relevant experimental results.

1) **Use small N_{tap} (such as 2):** FleXOR should be able to select the best out of $2^{N_{in}}$ possible outputs that are randomly selected from larger $2^{N_{out}}$ search space. Encryption performance of XOR gates is determined by randomness of $2^{N_{in}}$ output candidates, and is enhanced by increasing Hamming distance that is achieved by large N_{out} . Now, let N_{tap} be the number of 1’s in a row of M^\oplus . Another method to enhance encryption performance is to increase N_{tap} so as to increase the number of shuffles (through more XOR operations) using encrypted bits to generate quantized bits such that correlation between quantized bits is reduced. Large N_{tap} , however induces vanishing gradient problems in Eq. (5) or increased approximation error in Eq. (6). Hence, in practice, FleXOR training with small N_{tap} converges well with high test accuracy. Studying a training algorithm to understand a complex XOR-gate network with large N_{tap} would be an interesting research topic that is beyond the scope of this work. Subsequently, we show experimental results using $N_{tap}=2$ in the remainder of this paper.

2) **Use ‘tanh’ rather than STE for XOR:** Since forward propagation for a XOR gate only needs a sign function, the STE method is also applicable to XOR-gate gradient calculations. Another alternative method to model an XOR gate is to use Eq. (3) for both forward and backward propagation as if the XOR is modeled in an analog manner (then, real number XOR outputs are quantized through STE). We compare three different XOR modeling schemes in Figure 5 with test accuracy

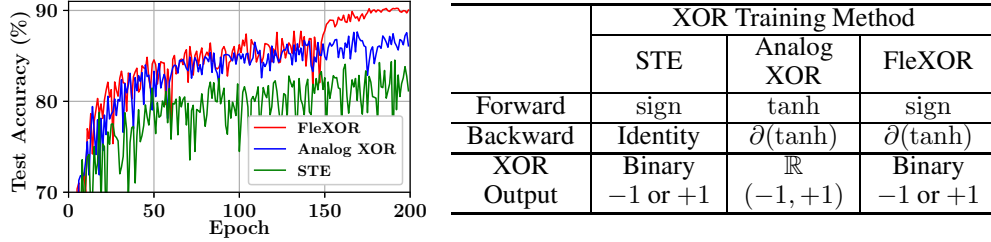


Figure 5: Test accuracy comparison on ResNet-32 (for CIFAR-10) using various XOR training methods. $N_{out}=10$, $N_{in}=8$, $q=1$ (thus, 0.8bit/weight), and $S_{\tanh}=10$.

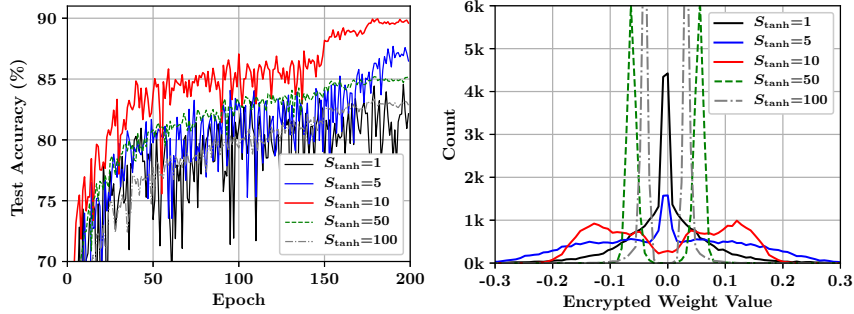


Figure 6: Test accuracy and distribution of encrypted weights (at the end of training) of ResNet-32 on CIFAR-10 using various S_{\tanh} and the same N_{out} , N_{in} , and q as Figure 5.

measured when encrypted weights and XOR gates are converted to be binary for inference. FleXOR training method shows the best result because a) sign function for forward propagation enables estimating the impact of binary XOR computations on the loss function and b) $\partial(\tanh)$ for backward propagation approximates the Heaviside step function better compared to STE. Note that limited gradients from the tanh function eliminate the need for weight clipping, which is often required for quantization-aware training schemes [3, 27].

3) **Optimize S_{\tanh} :** S_{\tanh} controls the smoothness of the tanh function for near-zero inputs. Large S_{\tanh} employs large gradient for small inputs and, hence, results in well-clustered encrypted weight values as shown in Figure 6. Too large of a S_{\tanh} , however, hinders encrypted weights from being finely-tuned through training. For FleXOR, S_{\tanh} is a hyper-parameter to be optimized.

4) **Learning rate and S_{\tanh} warmup:** Learning rate starts from 0 and linearly increases to reach the initial learning rate at a certain epoch as a warmup. Learning rate warmup is a heuristic scheme, but being widely accepted to improve generalization capability mainly by avoiding large learning rate in the initial phase [11, 8]. Similarly, S_{\tanh} starts from 5 to linearly increases to 10 using the same warmup schedule of the learning rate.

5) **Try various q , N_{in} , and N_{out} :** Using a warmup scheme for 100 epochs and learning rate decay by 50% at the 350th, 400th, and 450th epoch, Figure 7 presents test accuracy of ResNet-32 with various q , N_{in} , and N_{out} . For $q>1$, different M^\oplus configurations are constructed and then shared across all layers. Note that even for the 0.4bit/weight configuration (using $q=1$, $N_{in}=8$, and $N_{out}=20$), high accuracy close to 89% is achieved. 0.8bit/weight can be achieved by two different configurations (as shown on the right side of Figure 7) using ($q=1$, $N_{in}=8$, $N_{out}=10$) or ($q=2$, $N_{in}=8$, $N_{out}=20$). Interestingly, those two configurations show almost the same test accuracy, which implies that FleXOR is able to provide a linear relationship between the amount of encrypted weights and model accuracy (regardless of internal configurations). In general, lowering q reduces the amount of computations with quantized weights and a high N_{out} value is necessary for very low number of bits per weight since N_{in} also needs to be high enough to increase the Hamming distance.

We compare quantization results of ResNet-20 and ResNet-32 on CIFAR-10 using different compression schemes in Table 1 (with full-precision activation). BWN [22], BinaryRelax [28], and LQ-Net [29] propose different training algorithms for the same quantization scheme (i.e., binary

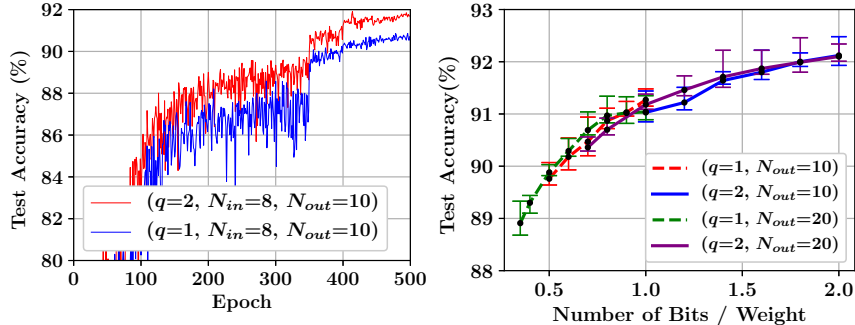


Figure 7: Test accuracy of ResNet-32 on CIFAR10 using learning rate warmup and various q , N_{in} , and N_{out} . The results on the right side are obtained by 5 runs.

Table 1: Weight compression comparison of ResNet-20 and ResNet-32 on CIFAR-10. For FleXOR, we use warmup scheme, $S_{\tanh}=10$, and $N_{out}=20$.

	ResNet-20			ResNet-32		
	FP	Compressed	Diff.	FP	Compressed	Diff.
BWN (1 bit)	92.68%	87.44%	-5.24%	93.40%	89.49%	-4.51%
BinaryRelax (1 bit)	92.68%	87.82%	-4.86%	93.40%	90.65%	-2.80%
LQ-Net (1 bit)	92.10%	90.10%	-1.90%	-	-	-
DSQ (1 bit)	90.70%	90.24%	-0.56%	-	-	-
FleXOR (1.0 bit)	91.87%	90.44%	-1.47%	92.33%	91.36%	-0.97%
FleXOR (0.8 bit)		89.91%	-1.90%		91.20%	-1.13%
FleXOR (0.6 bit)		89.16%	-2.71%		90.43%	-1.90%
FleXOR (0.4 bit)		88.23%	-3.64%		89.61%	-2.72%

codes). The main idea of these methods is to minimize quantization error and to obtain gradients from full-precision weights while the loss function is aware of quantization. Because all of quantization schemes in Table 1 uses $q=1$ and binary codes, the amount of computations using quantized weights is the same. FleXOR, however, allows reduced memory footprint and bandwidth which are critical for energy-efficient inference designs [9, 1]. Note that even though achieving the best accuracy for 1.0 bit/weight is not the main purpose of FleXOR (e.g., XOR gate may be redundant for $N_{in}=N_{out}$), FleXOR shows the minimum accuracy drop for ResNet-20 and ResNet-32 as shown in Table 1.

While binary neural networks allow only 1-bit quantization as the minimum, FleXOR can assign any fractional quantization bits (less than 1) to different layers. Such a property is especially useful when some layers exhibit high redundancy and relatively less importance such that very low number of quantization bits do not degrade accuracy noticeably [4, 26]. To demonstrate mixed precision quantization (with all less than 1-bit) enabled by FleXOR, we conduct experiments with ResNet-20 on CIFAR-10 while employing three different XOR-gate structures (i.e. multiple configurations of M^\oplus are provided to different layer groups.). Table 2 shows that FleXOR with differently optimized M^\oplus for each layer group can achieve higher compression ratio with smaller storage footprint compared to the case of FleXOR associated with just one common M^\oplus configuration for all layers. When N_{out} is fixed to be 20 for all layers, due to varied importance of each group, small N_{in} is allowed for the third group (of layers with large number of parameters) while relatively large N_{in} is selected for small layers. Compared to the case of $N_{in}=12$ for all layers (with 0.6 bits/weights), adaptively chosen N_{in} sets (i.e., 19 for layer 2-7, 16 for layer 8-13, and 7 for layer 14-19) yield higher accuracy (by 0.13%) and smaller bits/weights (by 0.13 bits/weights). As such, **FleXOR facilitates a fine-grained exploration of optimal quantization bit search** (given as fractional numbers determined by N_{in} , N_{out} , and q) that has not been available in the previous binary-coding-based quantization methods.

Table 2: ResNet-20 quantized by FleXOR with various M^\oplus assigned to layers ($N_{out}=20$ for all layers). We divide 20 layers into three groups of layers except for the first and last layers.

N_{in} (Bits/Weight)			Average Bits/Weight	Accuracy
Layer 2–7 (13.5k params)	Layer 8–13 (45k params)	Layer 14–19 (180k params)		
Fixed to be 12 (0.60)			0.60	89.16%
19 (0.95)	19 (0.95)	8 (0.40)	0.53	89.23% (+0.07)
16 (0.80)	16 (0.80)	8 (0.40)	0.50	89.19% (+0.03)
19 (0.95)	16 (0.80)	7 (0.35)	0.47	89.29% (+0.13)

Table 3: Weight compression comparison of ResNet-18 on ImageNet.

Methods	Bits/Weight	Top-1	Top-5	Storage Saving
Full Precision [10]	32	69.6%	89.2%	1×
BWN [22]	1	60.8%	83.0%	~ 32×
ABC-Net [20]	1	62.8%	84.4%	~ 32×
BinaryRelax [28]	1	63.2%	85.1%	~ 32×
DSQ [7]	1	63.7%	-	~ 32×
FleXOR ($N_{out} = 20$)	0.8	63.8%	84.8%	~ 40×
	0.63 (mixed) ²	63.3%	84.5%	~ 50.8×
	0.6	62.0%	83.7%	~ 53×

5 Experimental Results on ImageNet

In order to show that FleXOR principles can be extended to larger models, we choose ResNet-18 on ImageNet [23]. We use SGD optimizer with momentum of 0.9 and initial learning rate of 0.1. Batch size is 128, weight decay factor is 10^{-5} , and S_{\tanh} is 10. Learning rate is reduced by half at the 70th, 100th, and 130th. For warmup, during initial ten epochs, S_{\tanh} and learning rate increase linearly from 5 and 0.0, respectively, to initial values.

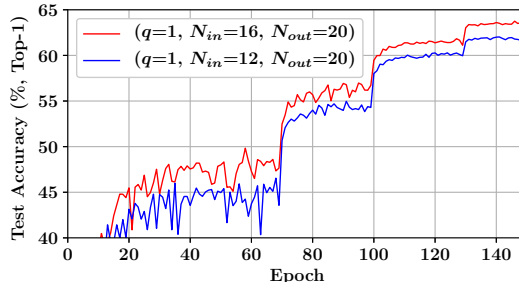


Figure 8: Test accuracy (Top-1) of ResNet-18 on ImageNet using FleXOR.

Figure 8 depicts the test accuracy of ResNet-18 on ImageNet when ($q=1$, $N_{in}=16$ and $N_{out}=20$) and ($q=1$, $N_{in}=12$ and $N_{out}=20$). Refer to Appendix for more results with $q=2$. Table 3 shows the comparison on model accuracy of ResNet-18 when weights are compressed by quantization (and additional encryption by FleXOR) while activations maintain full precision. Training ResNet-18 including FleXOR components is successfully performed. In Table 3, BinaryRelax and BWN do not modify the underlying model architecture, while ABC-Net introduces a new block structure of the convolution for quantized network designs. FleXOR achieves the best top-1 accuracy even with only 0.8bit/weight and demonstrates improved model accuracy as the number of bits per weight increases.

²To 4 groups of 3×3 conv layers in ResNet-18 (except the first conv layer connected to the inputs), we assign 0.9, 0.8, 0.7, and 0.6 bits/weight, respectively. To the remaining 1×1 conv layers (performing downsampling), we assign 0.95, 0.9, and 0.8 bits/weight, respectively.

6 Conclusion

This paper proposes an encryption algorithm/architecture, FleXOR, as a framework to further compress quantized weights. Encryption is designed to produce more outputs than inputs by increasing the Hamming distance of output functions when output functions are linear functions of inputs. Output functions are implemented as a combination of XOR gates which are included in the model to find encrypted and quantized weights through gradient descent while using the tanh function for backward propagation. FleXOR enables fractional numbers of bits for weights and, thus, much wider trade-offs between weight storage and model accuracy. Experimental results show that ResNet on CIFAR-10 and ImageNet can be represented by sub 1-bit/weight compression with high accuracy.

References

- [1] D. Ahn, D. Lee, T. Kim, and J.-J. Kim. Double Viterbi: Weight encoding for high compression ratio and fast on-chip reconstruction for deep neural network. In *International Conference on Learning Representations (ICLR)*, 2019.
- [2] Y. Choi, M. El-Khamy, and J. Lee. Towards the limit of network quantization. In *International Conference on Learning Representations (ICLR)*, 2017.
- [3] M. Courbariaux, Y. Bengio, and J.-P. David. BinaryConnect: Training deep neural networks with binary weights during propagations. In *Advances in Neural Information Processing Systems*, pages 3123–3131, 2015.
- [4] Z. Dong, Z. Yao, A. Gholami, M. W. Mahoney, and K. Keutzer. Hawq: Hessian aware quantization of neural networks with mixed-precision. In *Proceedings of the IEEE International Conference on Computer Vision*, pages 293–302, 2019.
- [5] J. Frankle and M. Carbin. The lottery ticket hypothesis: Finding sparse, trainable neural networks. In *International Conference on Learning Representations (ICLR)*, 2019.
- [6] R. Gong, X. Liu, S. Jiang, T. Li, P. Hu, J. Lin, F. Yu, and J. Yan. Differentiable soft quantization: Bridging full-precision and low-bit neural networks. *arXiv:1908.05033*, 2019.
- [7] R. Gong, X. Liu, S. Jiang, T. Li, P. Hu, J. Lin, F. Yu, and J. Yan. Differentiable soft quantization: Bridging full-precision and low-bit neural networks. In *Proceedings of the IEEE International Conference on Computer Vision*, pages 4852–4861, 2019.
- [8] A. Gotmare, N. S. Keskar, C. Xiong, and R. Socher. A closer look at deep learning heuristics: Learning rate restarts, warmup and distillation. In *International Conference on Learning Representations (ICLR)*, 2019.
- [9] S. Han, H. Mao, and W. J. Dally. Deep compression: Compressing deep neural networks with pruning, trained quantization and Huffman coding. In *International Conference on Learning Representations (ICLR)*, 2016.
- [10] K. He, X. Zhang, S. Ren, and J. Sun. Deep residual learning for image recognition. *2016 IEEE Conference on Computer Vision and Pattern Recognition (CVPR)*, pages 770–778, 2016.
- [11] T. He, Z. Zhang, H. Zhang, Z. Zhang, J. Xie, and M. Li. Bag of tricks to train convolutional neural networks for image classification. In *The IEEE Conference on Computer Vision and Pattern Recognition (CVPR)*, 2018.
- [12] S. Jung, C. Son, S. Lee, J. Son, J.-J. Han, Y. Kwak, S. J. Hwang, and C. Choi. Learning to quantize deep networks by optimizing quantization intervals with task loss. In *Proceedings of the IEEE Conference on Computer Vision and Pattern Recognition*, pages 4350–4359, 2019.
- [13] J. Kahn, G. Kalai, and N. Linial. The influence of variables on boolean functions. In *Proceedings of the 29th Annual Symposium on Foundations of Computer Science, SFCS '88*, pages 68–80, 1988.
- [14] A. Krizhevsky, G. Hinton, et al. Learning multiple layers of features from tiny images. Technical report, Citeseer, 2009.
- [15] S. J. Kwon, D. Lee, B. Kim, P. Kapoor, B. Park, and G.-Y. Wei. Structured compression by weight encryption for unstructured pruning and quantization. In *Proceedings of the IEEE/CVF Conference on Computer Vision and Pattern Recognition*, pages 1909–1918, 2020.

- [16] F. Lahoud, R. Achanta, P. Márquez-Neila, and S. Süsstrunk. Self-binarizing networks. *arXiv:1902.00730*, 2019.
- [17] D. Lee, D. Ahn, T. Kim, P. I. Chuang, and J.-J. Kim. Viterbi-based pruning for sparse matrix with fixed and high index compression ratio. In *International Conference on Learning Representations (ICLR)*, 2018.
- [18] F. Li and B. Liu. Ternary weight networks. *arXiv:1605.04711*, 2016.
- [19] H. Li, S. De, Z. Xu, C. Studer, H. Samet, and T. Goldstein. Training quantized nets: A deeper understanding. In *Advances in Neural Information Processing Systems*, pages 5813–5823, 2017.
- [20] X. Lin, C. Zhao, and W. Pan. Towards accurate binary convolutional neural network. In *Advances in Neural Information Processing Systems*, pages 345–353, 2017.
- [21] A. Polino, R. Pascanu, and D. Alistarh. Model compression via distillation and quantization. In *International Conference on Learning Representations (ICLR)*, 2018.
- [22] M. Rastegari, V. Ordonez, J. Redmon, and A. Farhadi. XNOR-Net: Imagenet classification using binary convolutional neural networks. In *ECCV*, 2016.
- [23] O. Russakovsky, J. Deng, H. Su, J. Krause, S. Satheesh, S. Ma, Z. Huang, A. Karpathy, A. Khosla, M. Bernstein, A. C. Berg, and L. Fei-Fei. ImageNet Large Scale Visual Recognition Challenge. *International Journal of Computer Vision (IJCV)*, 115(3):211–252, 2015. doi: 10.1007/s11263-015-0816-y.
- [24] P. Stock, A. Joulin, R. Gribonval, B. Graham, and H. Jégou. And the bit goes down: Revisiting the quantization of neural networks. *arXiv:1907.05686*, 2019.
- [25] N. A. Toubia. Survey of test vector compression techniques. *IEEE Design & Test of Computers*, 23: 294–303, 2006.
- [26] K. Wang, Z. Liu, Y. Lin, J. Lin, and S. Han. Haq: Hardware-aware automated quantization with mixed precision. In *Proceedings of the IEEE Conference on Computer Vision and Pattern Recognition*, pages 8612–8620, 2019.
- [27] C. Xu, J. Yao, Z. Lin, W. Ou, Y. Cao, Z. Wang, and H. Zha. Alternating multi-bit quantization for recurrent neural networks. In *International Conference on Learning Representations (ICLR)*, 2018.
- [28] P. Yin, S. Zhang, J. Lyu, S. Osher, Y. Qi, and J. Xin. Binaryrelax: A relaxation approach for training deep neural networks with quantized weights. *SIAM Journal on Imaging Sciences*, 11(4):2205–2223, 2018.
- [29] D. Zhang, J. Yang, D. Ye, and G. Hua. Lq-nets: Learned quantization for highly accurate and compact deep neural networks. In *Proceedings of the European Conference on Computer Vision (ECCV)*, pages 365–382, 2018.
- [30] C. Zhu, S. Han, H. Mao, and W. J. Dally. Trained ternary quantization. In *International Conference on Learning Representations (ICLR)*, 2017.

A Example of a XOR-gate Network Structure Representation

In Figure 2, outputs of a XOR-gate network are given as

$$\begin{aligned} y_1 &= x_1 \oplus x_3 \oplus x_4 \\ y_2 &= x_1 \oplus x_2 \\ y_3 &= x_1 \oplus x_2 \oplus x_3 \\ y_4 &= x_3 \oplus x_4 \\ y_5 &= x_2 \oplus x_4 \\ y_6 &= x_2 \oplus x_3 \oplus x_4. \end{aligned}$$

Equivalently, the same structure as above can be represented in a matrix as

$$\mathbf{M}^{\oplus} = \begin{bmatrix} 1 & 0 & 1 & 1 \\ 1 & 1 & 0 & 0 \\ 1 & 1 & 1 & 0 \\ 0 & 0 & 1 & 1 \\ 0 & 1 & 0 & 1 \\ 0 & 1 & 1 & 1 \end{bmatrix}. \quad (7)$$

Note that elements of \mathbf{M}^{\oplus} are matched with coefficients of $y_i (1 \leq i \leq 6)$. For two vectors $\mathbf{y} = \{y_1, y_2, y_3, y_4, y_5, y_6\}$ and $\mathbf{x} = \{x_1, x_2, x_3, x_4\}$, the following equation holds:

$$\mathbf{y} = \mathbf{M}^{\oplus} \cdot \mathbf{x}, \quad (8)$$

where element-wise addition and multiplication are performed by ‘XOR’ and ‘AND’ function, respectively. In Eq. (7), N_{tap} (i.e., the number of ‘1’s in a row) is 2 or 3.

B Supplementary Data for Basic FleXOR Training Principles

A Boolean XOR gate can be modeled as $\mathcal{F}^{\oplus}(x_1, x_2) = (-1) \text{sign}(x_1) \text{sign}(x_2)$ if 0 is replaced with -1 as shown in Table 4.

$\text{sign}(x_1)$	$\text{sign}(x_2)$	$\mathcal{F}^{\oplus}(x_1, x_2)$
-1	-1	-1
-1	+1	+1
+1	-1	+1
+1	+1	-1

Table 4: An XOR gate modeling using $\mathcal{F}^{\oplus}(x_1, x_2)$.

In Eq. (7), forward propagation for y_3 is expressed as

$$y_3 = \mathcal{F}^{\oplus}(x_1, x_2, x_3) = (-1)^2 \text{sign}(x_1) \text{sign}(x_2) \text{sign}(x_3). \quad (9)$$

while partial derivative of y_3 with respect to x_1 is given as (not derived from Eq. (9))

$$\frac{\partial y_3}{\partial x_1} = S_{\tanh}(-1)^2(1 - \tanh^2(x_1 \cdot S_{\tanh})) \tanh(x_2 \cdot S_{\tanh}) \tanh(x_3 \cdot S_{\tanh}), \quad (10)$$

or as

$$\frac{\partial y_3}{\partial x_1} \approx S_{\tanh}(-1)^2(1 - \tanh^2(x_1 \cdot S_{\tanh})) \text{sign}(x_2) \text{sign}(x_3). \quad (11)$$

We choose Eq. (11), instead of Eq. (10), as explained in Section 3.

As shown in Figure 9, large S_{\tanh} yields sharp transitions for near-zero inputs. Such a sharp approximation of the Heaviside step function produces large gradient values for small inputs and encourages encrypted weights to be separated into negative or positive values. Too large S_{\tanh} , however, has the same issues of a too large learning rate.

Figure 12 presents training loss and test accuracy when $N_{tap}=2$ and N_{out} is 10 or 20. Compared with Figure 5, $N_{tap}=2$ presents improved accuracy for the cases of high compression configurations (e.g., $N_{in}=4$ and $N_{out}=10$). We use $N_{tap} = 2$ for CIFAR-10 and ImageNet, since low N_{tap} avoids gradient vanishing problems or high approximation errors in Eq.(5) or Eq.(6).

Figure 13 plots the distribution of encrypted weights at different training steps when each row of \mathbf{M}^{\oplus} is randomly assigned with $\{0, 1\}$ (i.e., N_{tap} is $N_{in}/2$ on average) or assigned with only two 1’s ($N_{tap}=2$). Due to gradient calculations based on tanh and high S_{\tanh} , encrypted weights tend to be clustered on the left or right (near-zero encrypted weights become less as N_{tap} increases) even without weight clipping.

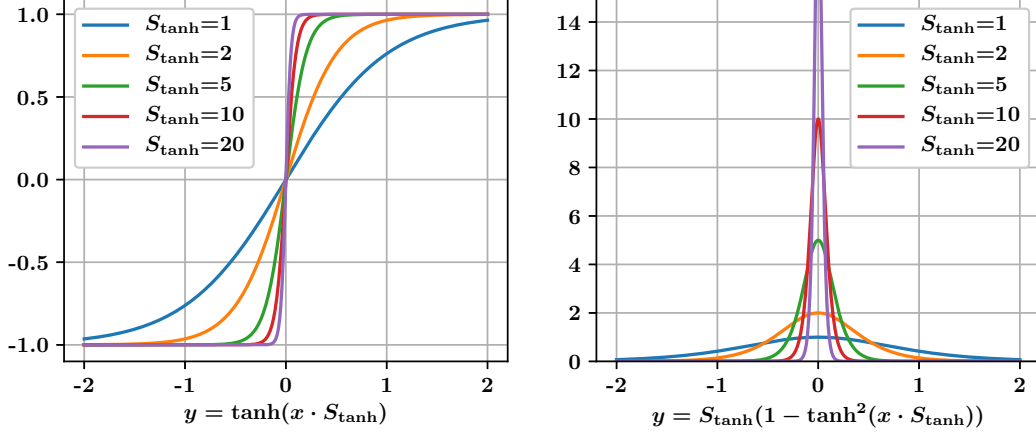


Figure 9: The left graph shows hyperbolic tangent ($y = \tanh(x \cdot S_{\tanh})$) graphs with various scaling factors (S_{\tanh}). The right graph shows their derivatives. These graphs support the arguments of ‘Optimize S_{\tanh} ’ in Section 4.

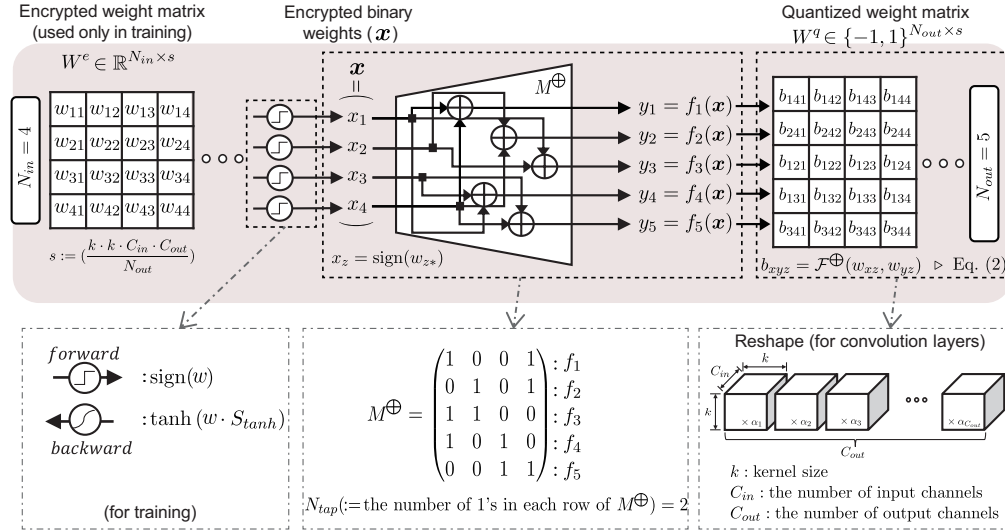


Figure 10: An example showing FleXOR operations for training. XOR gates are described in different ways for forward- and backward propagation. Once we obtain encrypted binary weights after training, we use digital XOR gates for inference.

C Supplementary Experimental Results of CIFAR-10 and ImageNet

In this section, we additionally provide various graphs and accuracy tables for ResNet models on CIFAR10 and ImageNet. We also present experimental results from wider hyper-parameters searches including $q=2$ with two separate M^{\oplus} configurations (with the same N_{in} and N_{out} for two M^{\oplus} matrices).

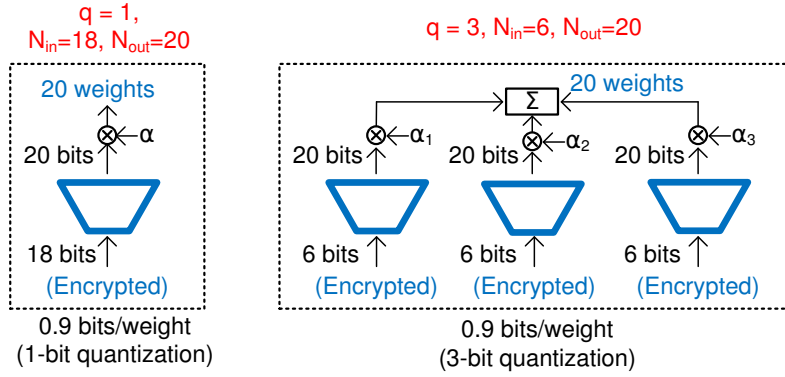


Figure 11: Using the same weight storage footprint, FleXOR enables various internal quantization schemes. (Left): 1-bit internal quantization. (Right): 3-bit internal quantization with 3 different M^\oplus configurations.

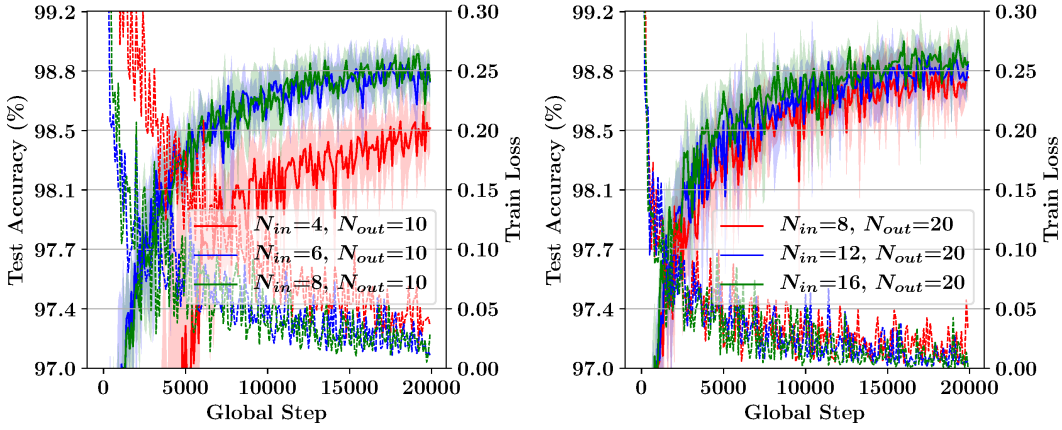


Figure 12: Test accuracy and training loss of LeNet-5 on MNIST when number of ‘1’s in each row of M^\oplus is fixed to be 2 ($N_{tap}=2$). N_{out} is 10 or 20 to generate, effectively, 0.4, 0.6, or 0.8 bit/weight quantization. With low N_{tap} of M^\oplus , MNIST training presents less variations on training loss and test accuracy that in Figure 5.

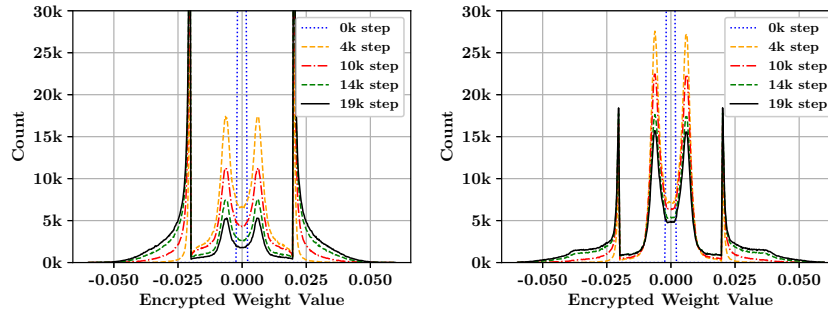


Figure 13: Distribution of encrypted weight values for FC1 layer of LeNet-5 at different training steps using $S_{tanh}=100$ and $N_{out}=10$. (Left): M^\oplus is randomly filled ($N_{tap} \approx N_{in}/2$). (Right): $N_{tap} = 2$ for every row of M^\oplus .

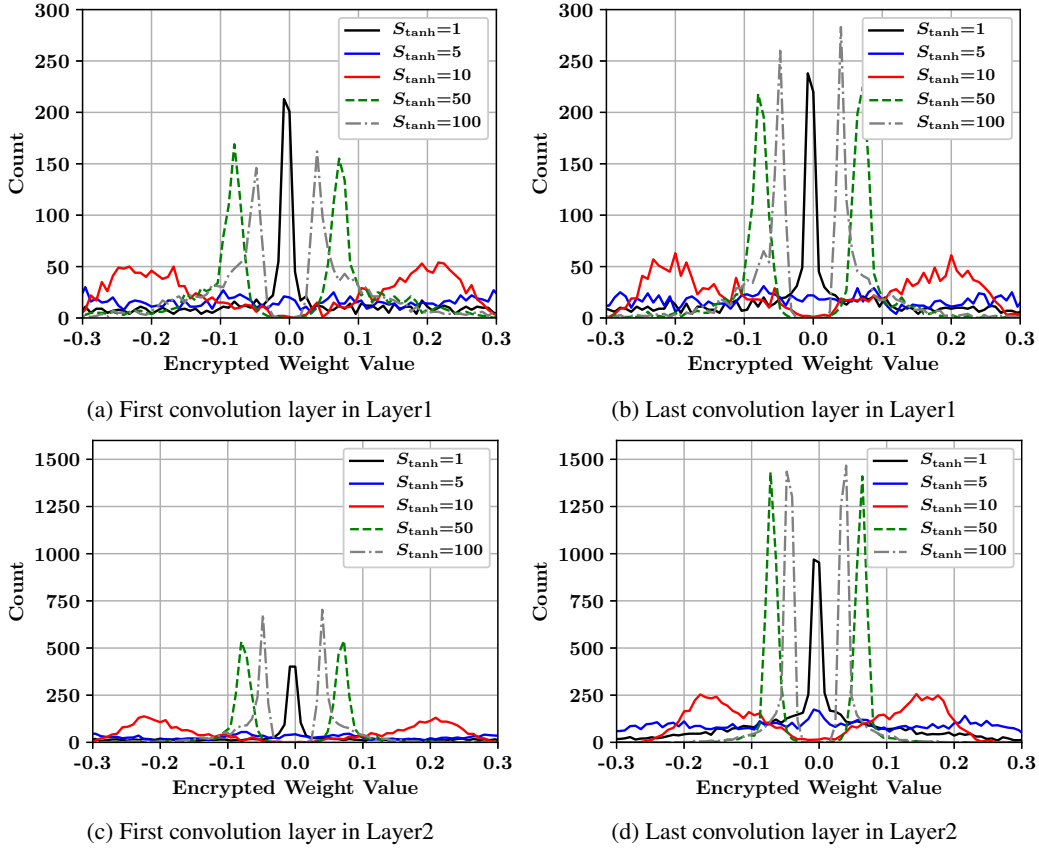
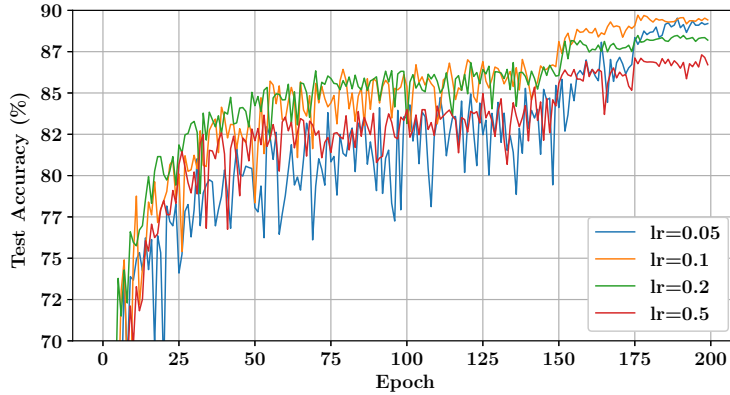


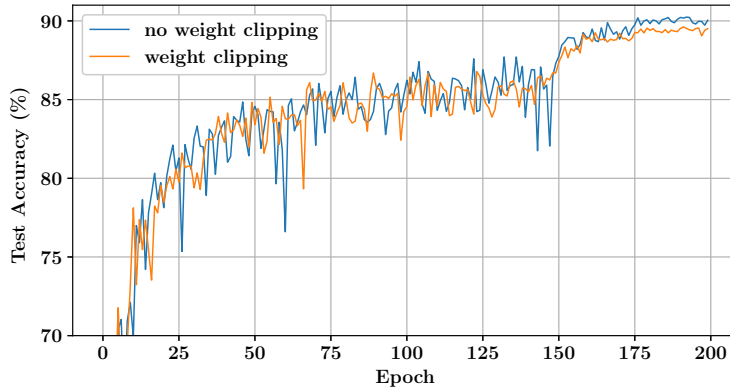
Figure 14: Distributions of encrypted weights (at the end of training) in various layers of ResNet-32 on CIFAR-10 using various S_{\tanh} and the same N_{out} , N_{in} , and q as Figure 7. The ResNet-32 network mainly consists of three layers according to the feature map sizes: Layer1, Layer2 and Layer3.

	Bits/Weight	ResNet-20		ResNet-32		Comp. Ratio
FP	32	91.87%	-	92.33%	-	1.0x
$N_{in}=10, N_{out}=10$	1.0	90.21%	-1.66%	91.40%	-0.93%	29.95×
$N_{in}=9, N_{out}=10$	0.9	90.03%	-1.84%	91.28%	-1.05%	31.82×
$N_{in}=8, N_{out}=10$	0.8	89.73%	-2.14%	90.96%	-1.37%	35.32×
$N_{in}=7, N_{out}=10$	0.7	89.88%	-1.99%	90.67%	-1.66%	39.68×
$N_{in}=6, N_{out}=10$	0.6	89.21%	-2.66%	90.41%	-1.92%	45.27×
$N_{in}=5, N_{out}=10$	0.5	88.59%	-3.28%	89.95%	-2.38%	52.70×

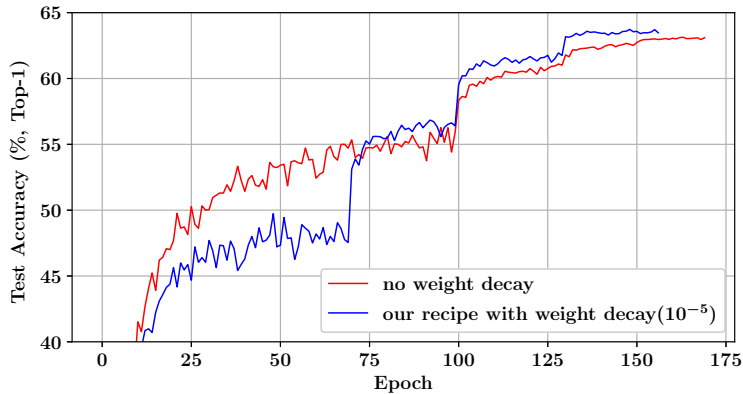
Table 5: Weight compression comparison of ResNet-20 and ResNet-32 on CIFAR-10 when $N_{out}=10$. Parameters and recipes not described in the table are the same as in Table 1. We also present compression ratio for fractional quantized ResNet-32 when one scaling factor (α) is assigned to each output channel.



(a) **Initial Learning Rate (0.1):** Test accuracy of ResNet-32 on CIFAR10 using the learning schedule in Figure 7 and various initial learning rates (0.05, 0.1, 0.2, 0.5).

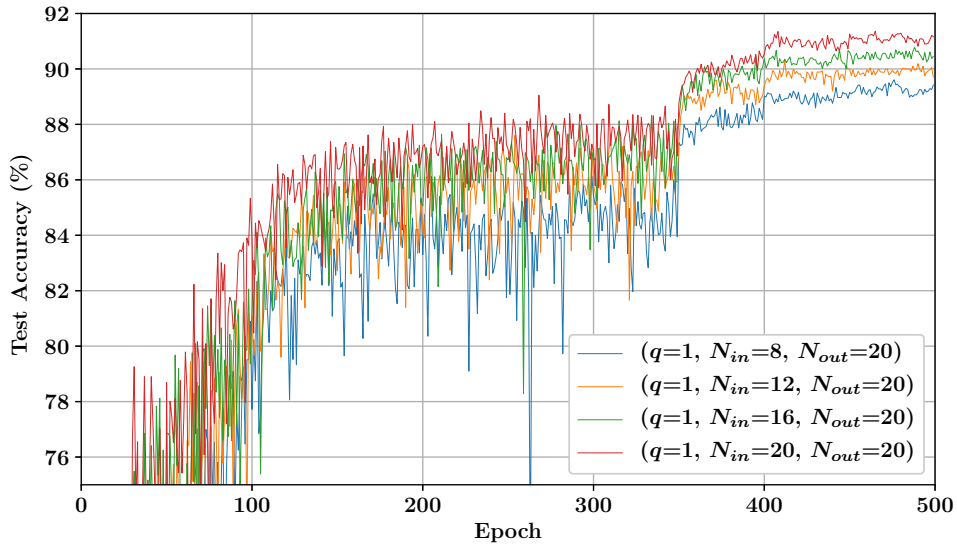


(b) **No Weight Clipping:** Test accuracy of ResNet-32 on CIFAR10 using the learning schedule in Figure 7. As for weight clipping, we restrict the encrypted weights to be ranged as $(-2.0/S_{\tanh}, +2.0/S_{\tanh})$. As can be observed, the red line implies that weight clipping is not effective with FleXOR.

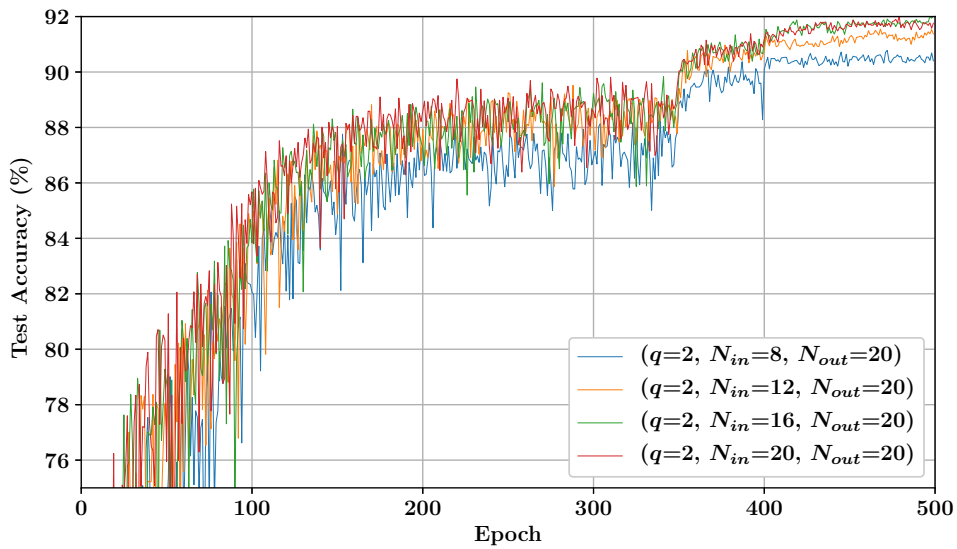


(c) **Weight Decay Factor (10⁻⁵):** Two graphs depict test accuracy of ResNet-18 on ImageNet with or without weight decay. The learning rate in the red line (no weight decay) is reduced by half at the 100th, 130th and 150th epochs. The learning rate of the blue line (with weight decay) is reduced by half at 70th, 100th and 130th epochs. With weight decay (blue graph), despite slow convergence in the early training steps, model accuracy is eventually higher than the red one without weight decay scheme.

Figure 15: Comparison of various hyper-parameter choices for CIFAR-10 or ImageNet.



(a) Test accuracy using $q=1$.



(b) Test accuracy using $q=2$. Compared to the above plots (Figure 16a), this figure shows that a combination of multiple M^\oplus for a binary code can lead to stable learning curves and higher model accuracy.

Figure 16: Test accuracy of ResNet-32 on CIFAR-10 using learning rate warmup (for 100 epochs) and $N_{out}=20$

	ResNet-20			ResNet-32		
	FP	Quant.	Diff.	FP	Quant.	Diff.
TWN (ternary)	92.68%	88.65%	-4.03%	93.40%	90.94%	-2.46%
BinaryRelax (ternary)	92.68%	90.07%	-1.91%	93.40%	92.04%	-1.36%
TTQ (ternary)	91.77%	91.13%	-0.64%	92.33%	92.37%	+0.04%
LQ-Net (2 bit)	92.10%	91.80%	-0.30%	-	-	-
FlexOR($q=2, N_{out}=20$)						
$N_{in}=20, 2.0$ bit/weight		91.38%	-0.49%		92.25%	-0.08%
$N_{in}=18, 1.8$ bit/weight		91.00%	-0.87%		92.27%	-0.06%
$N_{in}=16, 1.6$ bit/weight	91.87%	90.88%	-0.99%	92.33%	92.11%	-0.22%
$N_{in}=14, 1.4$ bit/weight		90.90%	-0.97%		92.02%	-0.31%
$N_{in}=12, 1.2$ bit/weight		90.56%	-1.31%		91.62%	-0.71%
FlexOR($q=2, N_{out}=10$)						
$N_{in}=10, 2.0$ bit/weight		91.19%	-0.68%		92.61%	+0.28%
$N_{in}=9, 1.8$ bit/weight		91.44%	-0.43%		92.09%	-0.24%
$N_{in}=8, 1.6$ bit/weight	91.87%	91.10%	-0.77%	92.33%	92.08%	-0.25%
$N_{in}=7, 1.4$ bit/weight		90.94%	-0.93%		91.74%	-0.59%
$N_{in}=6, 1.2$ bit/weight		90.56%	-1.31%		91.37%	-0.96%

Table 6: Weight compression comparison of ResNet-20 and ResNet-32 on CIFAR-10 using learning rate warmup (for 100 epochs) and $q=2$. As mentioned in Figure 6, multiple M^\oplus can be combined for multi-bit quantization schemes. Then, the number of scaling factors should be doubled. FlexOR with $q=2$ and two different M^\oplus structures achieve full-precision accuracy when both N_{in} and N_{out} are 10.

Methods	Bits/Weight	Top-1	Top-5
Full Precision [10]	32	69.6%	89.2%
TWN [18]	ternary	61.8%	84.2%
ABC-Net [20]	2	63.7%	85.2%
BinaryRelax [28]	ternary	66.5%	87.3%
TTQ(1.5× Wide) [30]	ternary	66.6%	87.2%
LQ-net [29]	2	68.0%	88.0%
QIL [12]	2	68.1%	88.3%
FlexOR ($q=2, N_{out}=20$)	1.6 (0.8×2)	66.2%	86.7%
	1.2 (0.6×2)	65.4%	86.0%
	0.8 (0.4×2)	63.8%	85.0%

Table 7: Weight compression comparison of ResNet-18 on ImageNet when $q=2$. Since q is 2, we also list the other compression schemes which use 2-bit or ternary quantization scheme for model compression.